Support Information

Amine-functionalized mesoporous silica-supported PdIr catalyst: boosting room-temperature hydrogen generation from formic acid

Wendan Nie,‡[a] Yixing Luo,‡[a] Qifeng Yang,[a] Gang Feng,[b] Qilu Yao,[a] and Zhang-Hui Lu[a]*

[a]*Institute of Advanced Materials (IAM), College of Chemistry and Chemical Engineering, Jiangxi Normal University, Nanchang 330022, China.*

[b]*College of Chemistry, Nanchang University, Nanchang 330031, China.*

‡These authors contributed equally.

*E-mail: luzh@jxnu.edu.cn

Table of Contents

Experimental Section

Synthesis of SBA-15

According to previous work,[S1] SBA-15 was prepared via a supramolecular self-assembly method. Typically, Pluronic® 123 (4.0 g) was dissolved in 94 mL deionized water, and stirred for 2 h at 313 K. Subsequently, HCl (20 mL) and TEOS (8.8 g) were added into above mixture, which was stirred continuously for 24 h at 313 K. The mixture was put into an autoclave and hydrothermally treated at 373 K for 24 h. Then white precipitate was collected by filtration, washed with copious amount of deionized water until neutral pH and dried at 333 K overnight. The organic template was removed by calcination at 823 K for 6 h to obtain the SBA-15 support.

Synthesis of SBA-15-NH_2

Functionalization of SBA-15 with amine groups was referring to a reported procedure.[S2] 1.0 g of SBA-15 was mixed with 6 mL of APTES in 60 mL of anhydrous toluene after treated at 378 K for 12 h. The resulting slurry was allowed to stir and reflux for 24 h at 353 K under the nitrogen atmosphere. The SBA-15-NH_2 was obtained as a white precipitate after washed with ethanol and dried at 313 K under vacuum overnight. In addition, to obtain varying -NH_2 groups loading on SBA-15, varying dosage of APTES (1.5 mL, 3 mL, 6 mL, 9 mL, and 12 mL) was added.

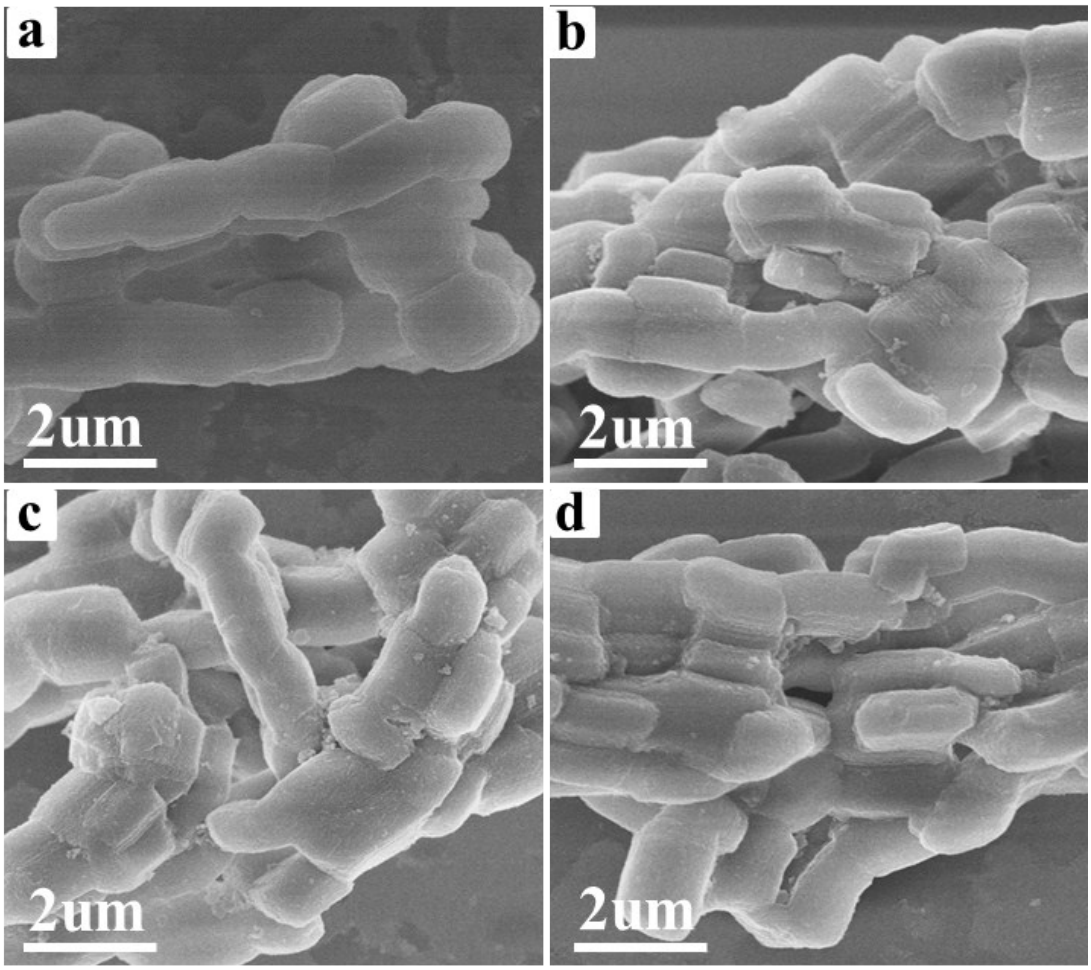

Figure S1. SEM images of the (a) SBA-15, (b) SBA-15-NH_2, (c) fresh-prepared $Pd_{0.85}Ir_{0.15}$/SBA-15-NH_2 NCs, and (d) $Pd_{0.85}Ir_{0.15}$/SBA-15-NH_2 NCs after reusability test.

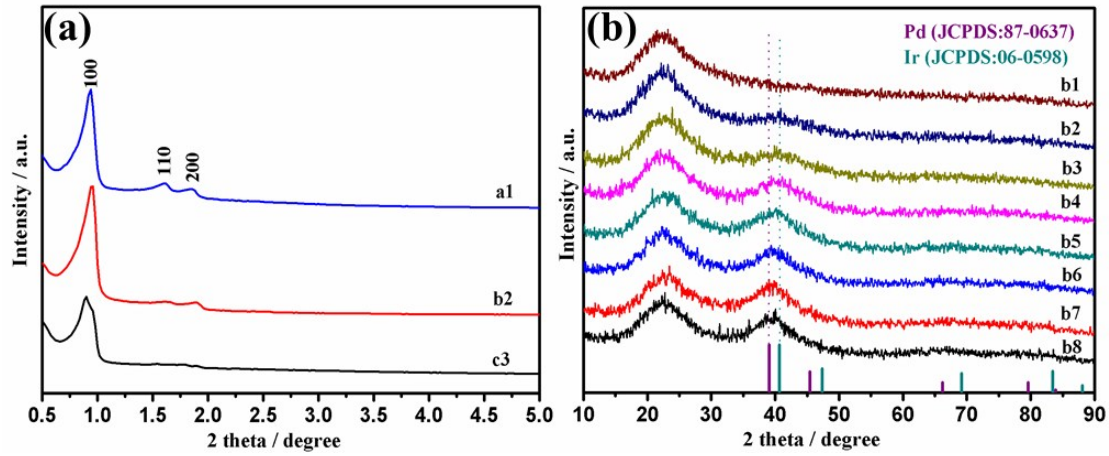

Figure S2. (a) Small-angle XRD patterns of (a1) SBA-15, (a2) SBA-15-NH_2, and (a3) $Pd_{0.85}Ir_{0.15}$/SBA-15-NH_2 NCs; (b) Wide-angle XRD patterns of (b1) Ir/SBA-15-NH_2, (b2) $Pd_{0.2}Ir_{0.8}$/SBA-15-NH_2, (b3) $Pd_{0.4}Ir_{0.6}$/SBA-15-NH_2, (b4) $Pd_{0.6}Ir_{0.4}$/SBA-15-NH_2, (b5) $Pd_{0.8}Ir_{0.2}$/SBA-15-NH_2, (b6) $Pd_{0.85}Ir_{0.15}$/SBA-15-NH_2, (b7) $Pd_{0.9}Ir_{0.1}$/SBA-15-NH_2, and (b8) Pd/SBA-15-NH_2 NCs.

X-ray diffraction (XRD) was applied to investigate the detailed crystal structure of the as-prepared specimens. Figure S2a shows the small-angle XRD patterns of the SBA-15, SBA-15-NH_2, and $Pd_{0.85}Ir_{0.15}$/SBA-15-NH_2 NCs. It can be seen that the three peaks at 2θ = 0.90°, 1.59°, and 1.89° are observed for all catalyst samples, which can be attributed to the (100), (110), and (200) planes of the ordered two-dimensional hexagonal mesoporous structure. Moreover, the framework of SBA-15 is maintained after the APTES functionalization and the loading of PdIr NPs, which agrees very well with the results measured by nitrogen adsorption-desorption isotherms (Figure 1) and FT-IR spectra (Figure 3a). The wide-angle XRD patterns (Figure S2b) shows that the strong and broad diffraction patterns at 2θ=15-35° can be attributed to the amorphous silica. Besides the diffraction of amorphous silica, the peaks between those of metallic Pd (111) (JCPDS: 87-0637) and Ir (111) (JCPDS: 06-0598) are also observed for the specimens, suggesting the formation of PdIr alloy structure.

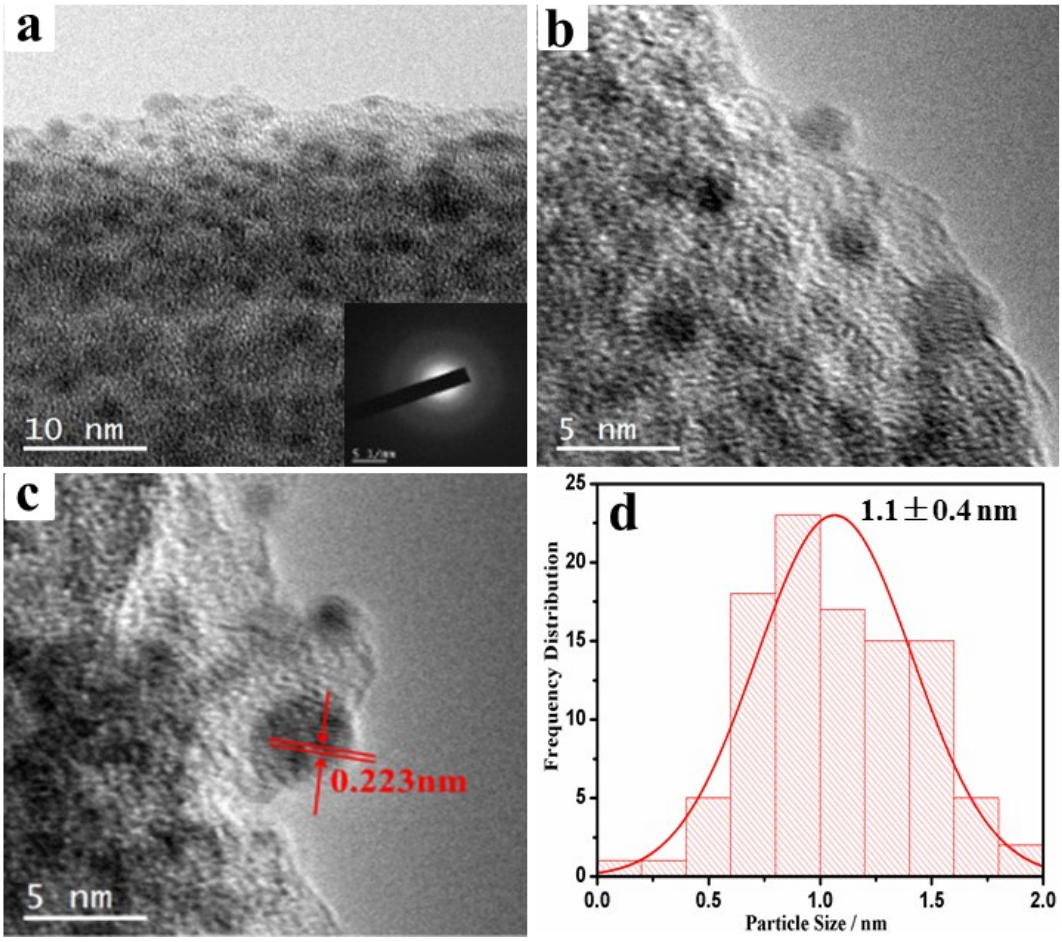

Figure S3. (a-c) High-resolution TEM images (inset of a) corresponding SAED pattern, and (d) particle distribution of the $Pd_{0.85}Ir_{0.15}$/SBA-15-NH_2 NCs.

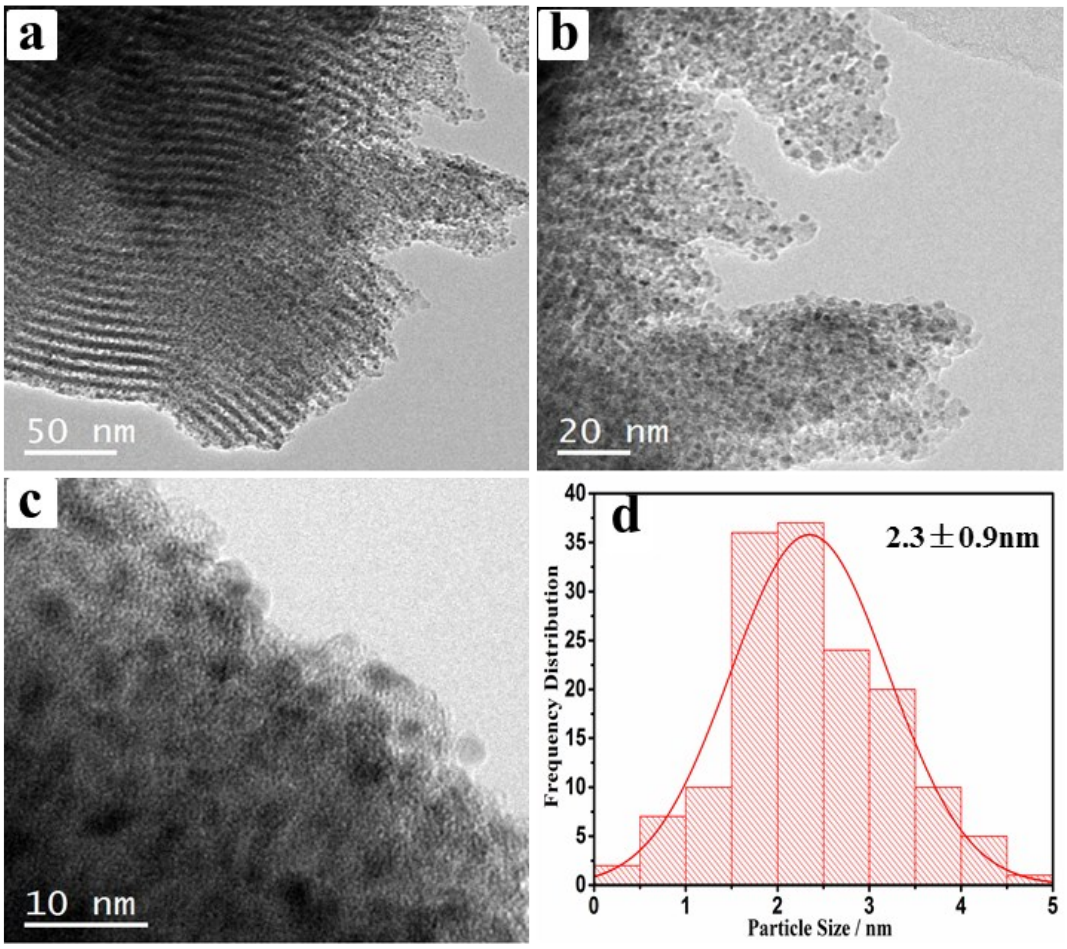

Figure S4. (a-c) TEM images and (d) particle distribution of Pd/SBA-15-NH_2 NCs.

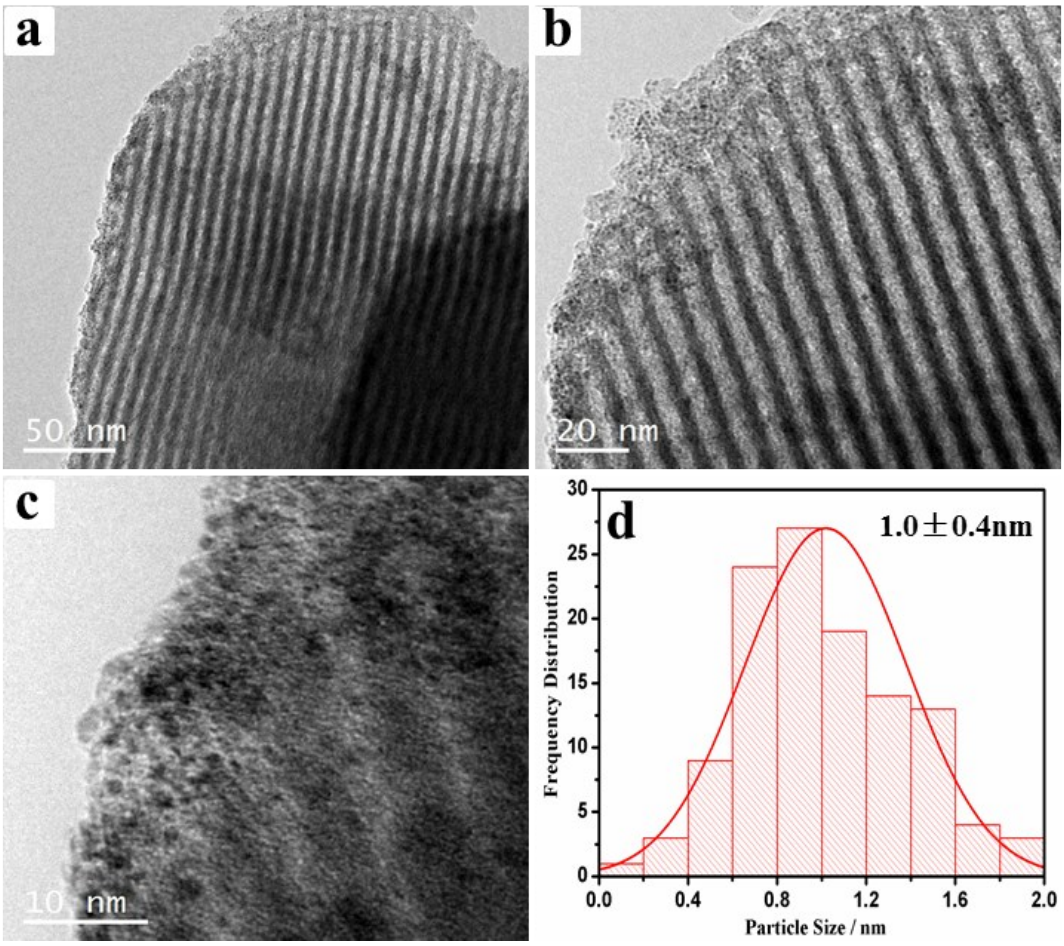

Figure S5. (a-c) TEM images and (d) particle distribution of Ir/SBA-15-NH_2 NCs.

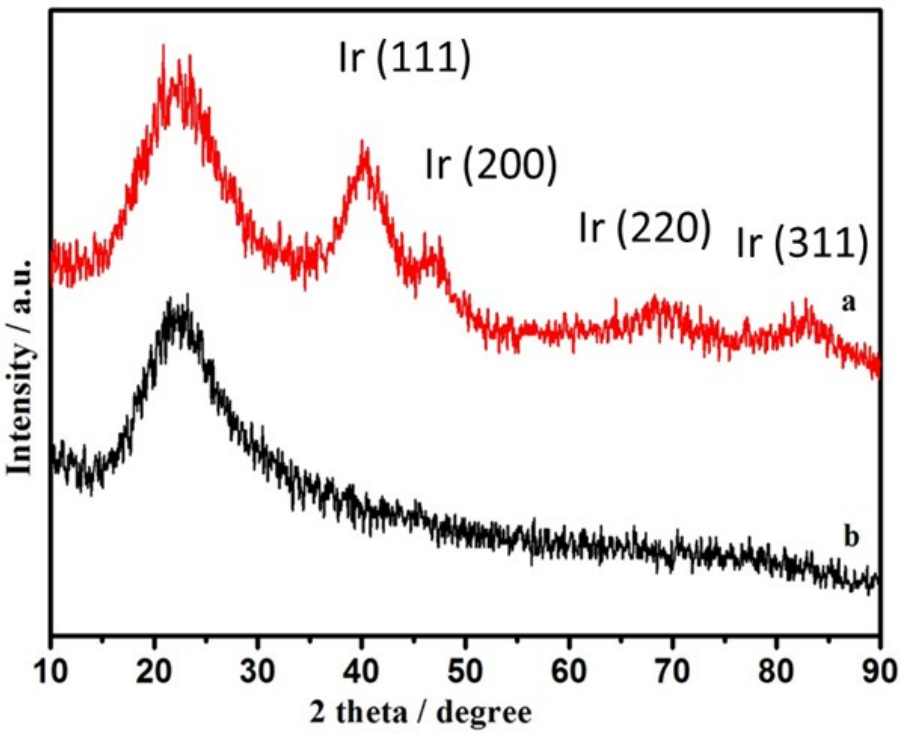

Figure S6. Wide-angle XRD patterns for the Ir/SBA-15-NH_2 NCs (a) after and (b) before treated at 823 K for 4 h in Ar atmosphere.

As shown in Figure S6, the diffraction peaks of metallic Ir was absent in the Ir/SBA-15-NH_2 NCs. It can be attributed to the high dispersion of Ir NPs on SBA-15-NH_2 with very small particle size and low crystallinity. The TEM images (Figure S5) confirmed that the Ir NPs are well dispersed on SBA-15-NH_2. After Ir/SBA-15-NH_2 NCs was treated at 823 K for 4 h in Ar atmosphere, the typically diffraction peaks of metallic Ir at 2θ = 40.6°, 47.3°, 69.14°, and 83.4° were appeared, and the peaks are indexed as (111), (200), (220), and (311) plans of metallic Ir (JCPDS: 06-0598), respectively.

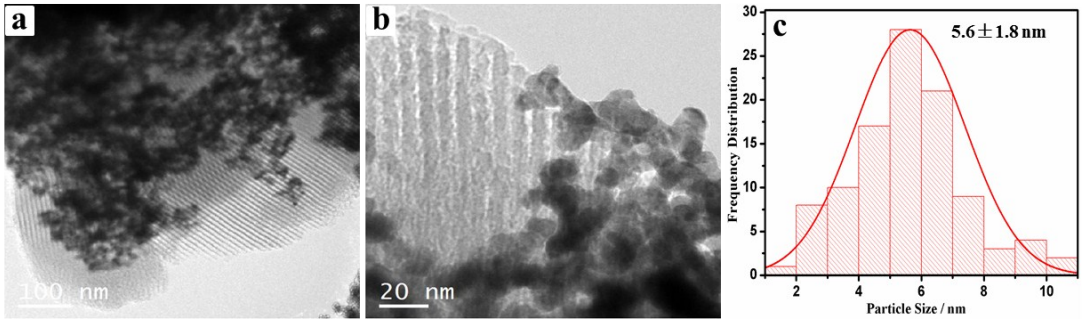

Figure S7. (a-b) TEM images and (c) particle distribution of $Pd_{0.85}Ir_{0.15}$/SBA-15 NCs.

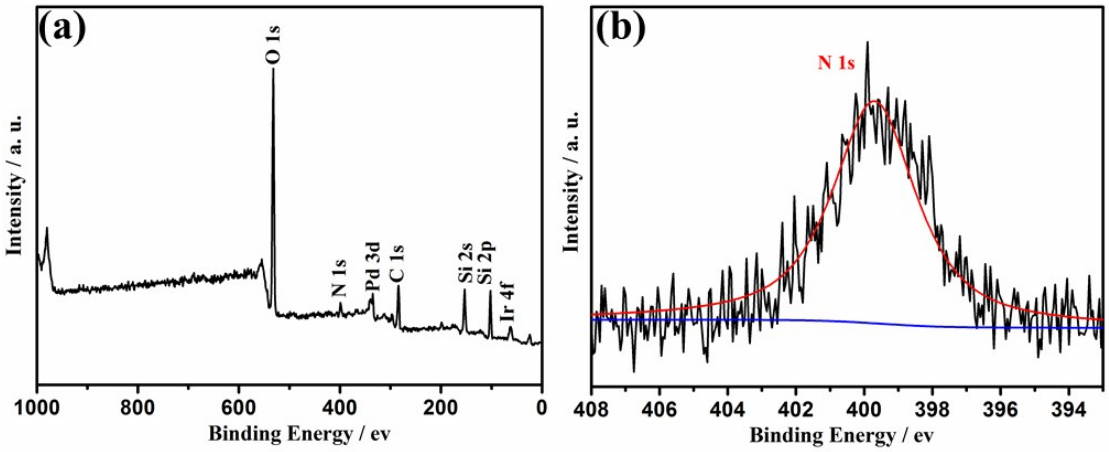

Figure S8. (a) The survey XPS spectrum of $Pd_{0.85}Ir_{0.15}$/SBA-15-NH_2 NCs and XPS spectra of N 1s in the $Pd_{0.85}Ir_{0.15}$/SBA-15-NH_2 NCs.

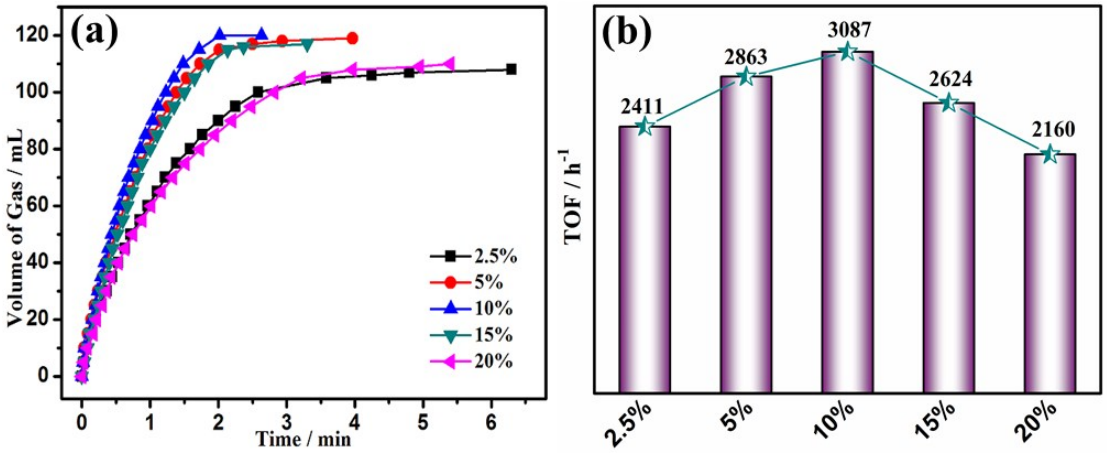

Figure S9. Volume of the generated gas (CO_2 + H_2) versus time for the dehydrogenation of FA in FA-SF aqueous solution over $Pd_{0.85}Ir_{0.15}$/SBA-15-NH_2 NCs (a) with different metal loadings at 298 K and (b) the corresponding initial TOF values (n_{PdIr}/n_{FA} = 0.02, FA/SF=1/3).

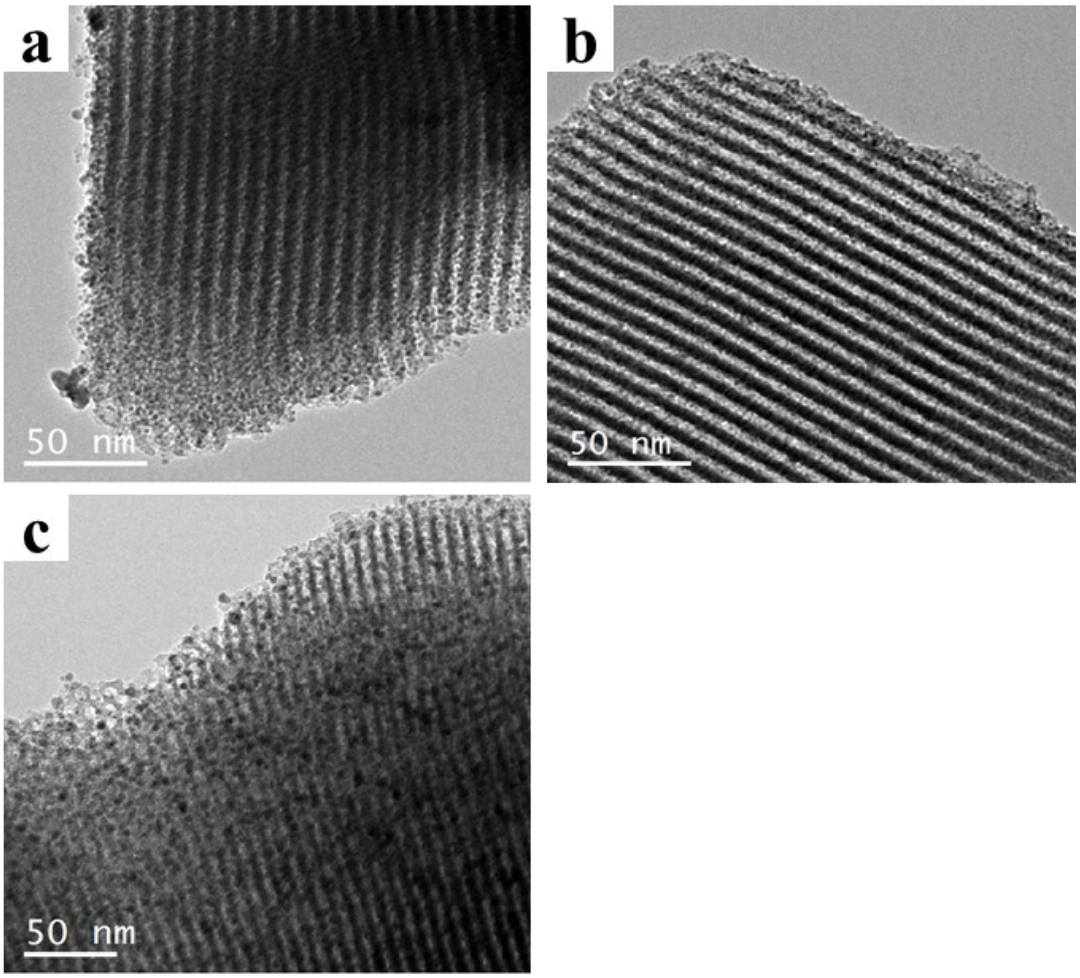

Figure S10. TEM images of $Pd_{0.85}Ir_{0.15}$/SBA-15 NCs with different PdIr loading (a) 5 wt%, (b) 10 wt% and (c) 20wt %.

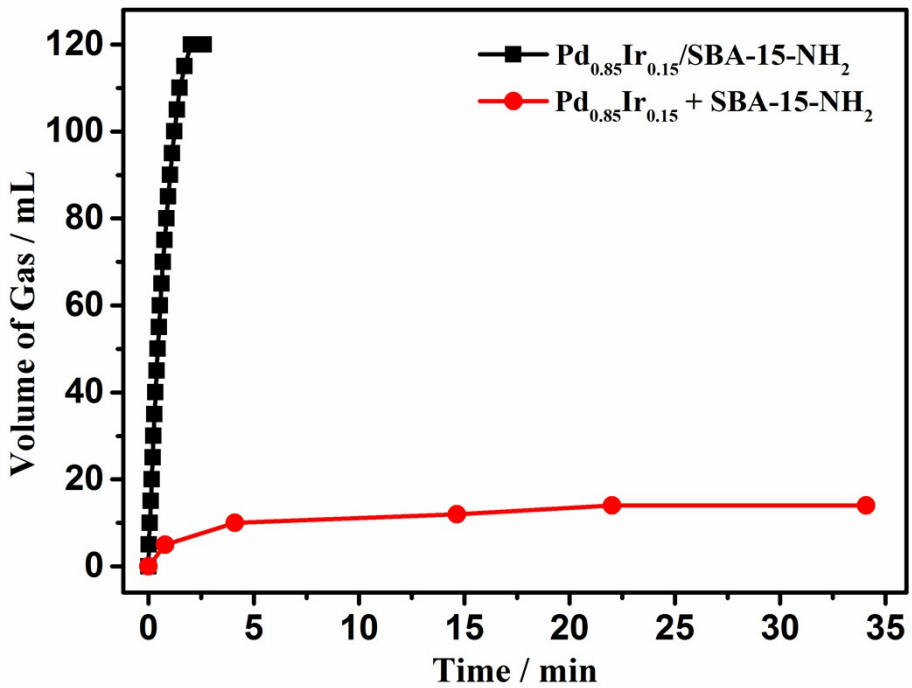

Figure S11. Volume of the generated gas (CO_2 + H_2) versus time for the dehydrogenation of FA in FA-SF aqueous solution over physical mixture of $Pd_{0.85}Ir_{0.15}$ and SBA-15-NH_2 and $Pd_{0.85}Ir_{0.15}$/SBA-15-NH_2 NCs at 298 K (n_{PdIr}/n_{FA} = 0.02, FA/SF=1/3, 10 wt%).

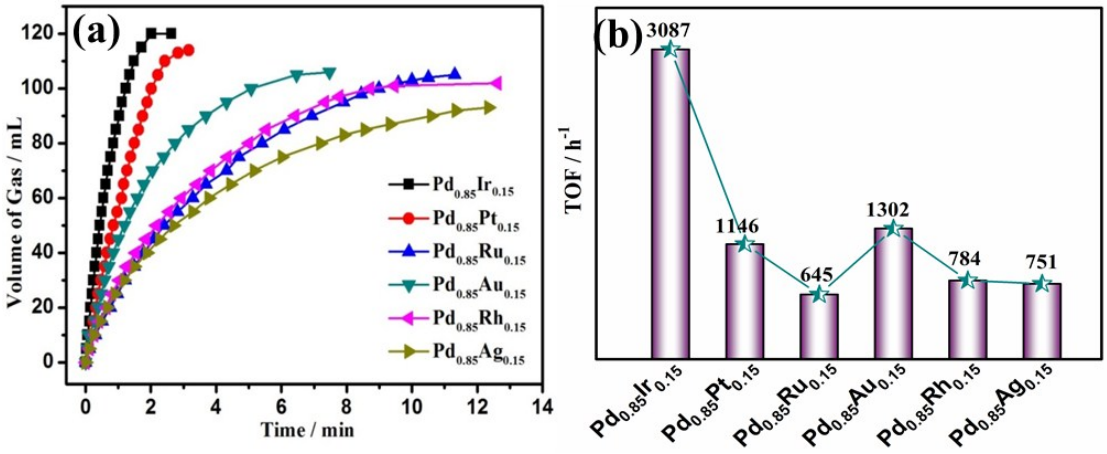

Figure S12. Volume of the generated gas (CO_2 + H_2) versus time for the dehydrogenation of FA in FA-SF aqueous solution over $Pd_{0.85}M_{0.15}$/SBA-15-NH_2 NCs (M = Ir, Pt, Ru, Au, Rh, and Ag) at 298 K and (b) the corresponding initial TOF value (n_{PdIr}/n_{FA} = 0.02, FA/SF=1/3, 10 wt%).

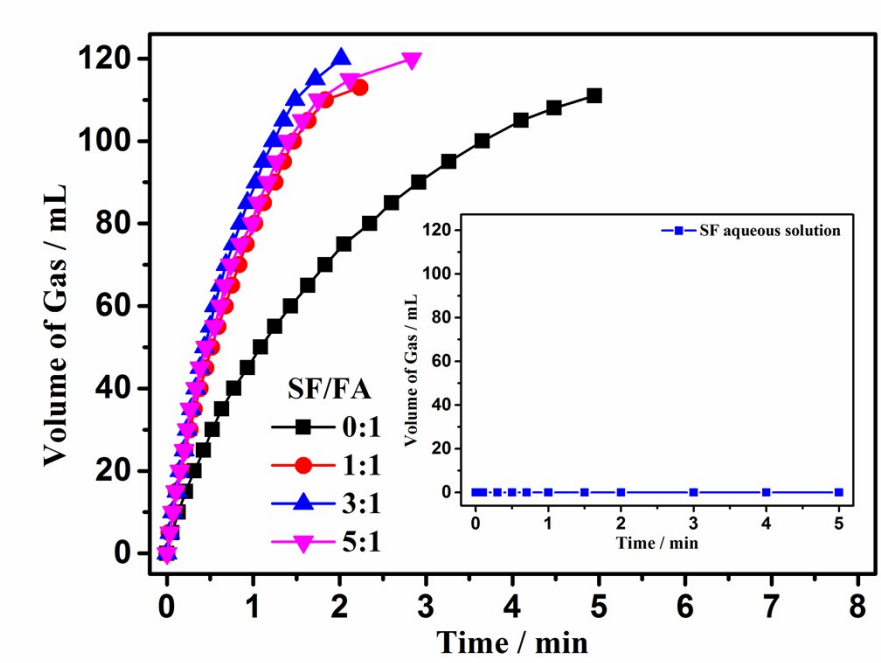

Figure S13. Volume of the generated gas (CO_2 + H_2) versus time for the dehydrogenation of FA in the presence of different SF/FA molar ratios and (inset) pure SF aqueous solution over $Pd_{0.85}Ir_{0.15}$/SBA-15-NH_2 NCs at 298 K (n_{PdIr}/n_{FA} = 0.02, 10 wt%).

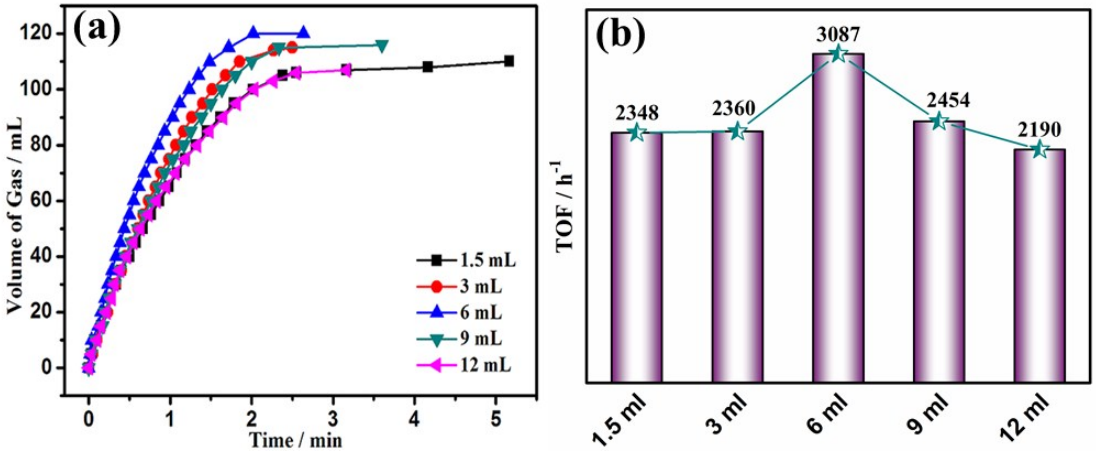

Figure S14. Volume of the generated gas (CO_2+H_2) versus time for the dehydrogenation of FA in FA-SF aqueous solution over $Pd_{0.85}Ir_{0.15}$/SBA-15-NH_2 NCs (a) with different volume of APTES at 298 K and (b) the corresponding initial TOF values (n_{PdIr}/n_{FA} = 0.02, FA/SF=1/3, 10 wt%).

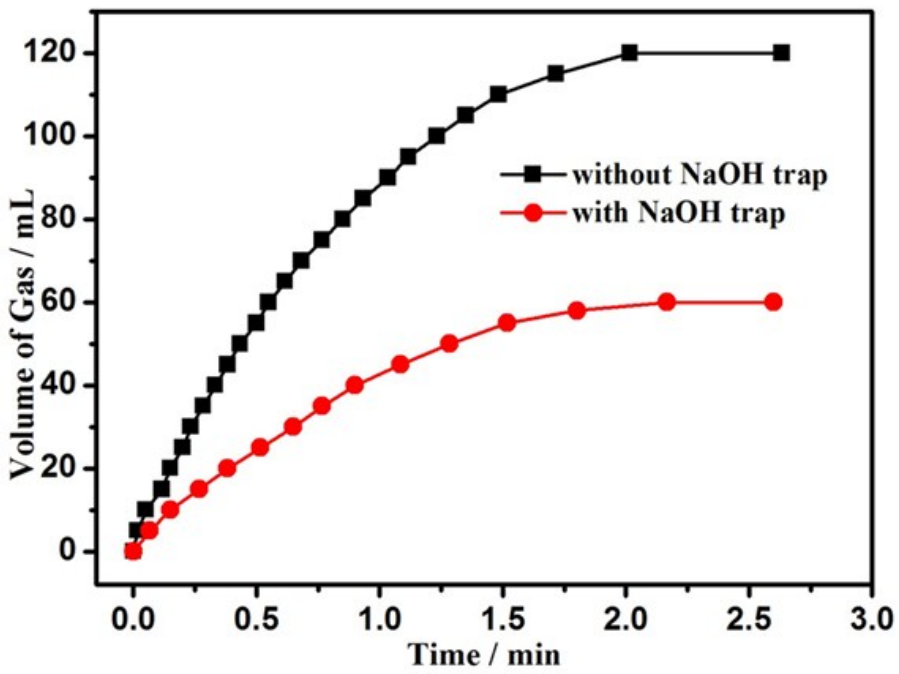

Figure S15. Volume of the generated gas (CO_2+H_2) versus time for the dehydrogenation of FA in FA-SF aqueous solution over $Pd_{0.85}Ir_{0.15}$/SBA-15-NH_2 NCs with/without NaOH trap at 298 K (n_{PdIr}/n_{FA} = 0.02, FA/SF=1/3, 10 wt%).

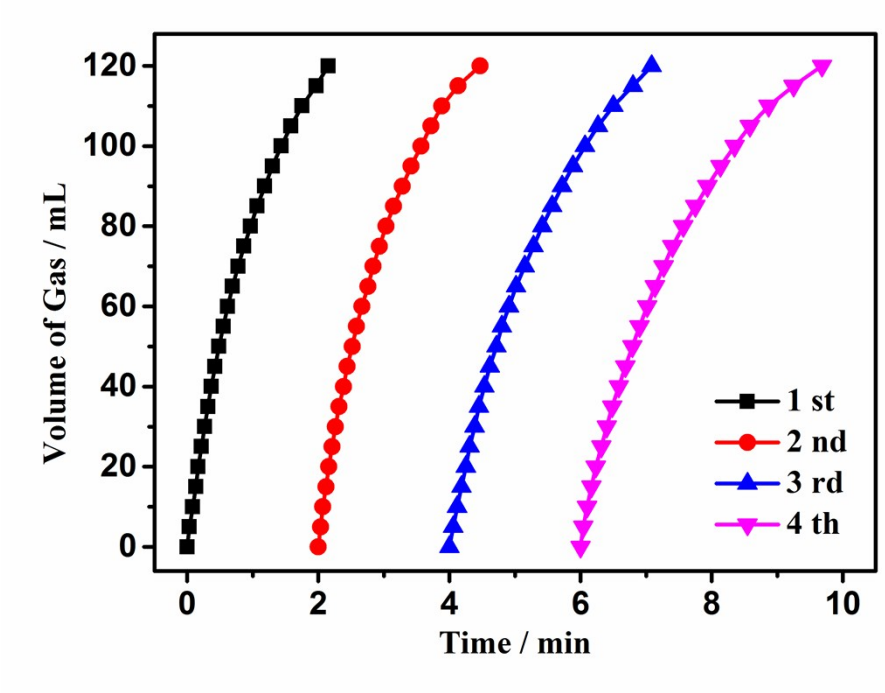

Figure S16. Reusability test of the optimized $Pd_{0.85}Ir_{0.15}$/SBA-15-NH_2 NCs for the dehydrogenation of FA in FA-SF aqueous solution at 298 K.

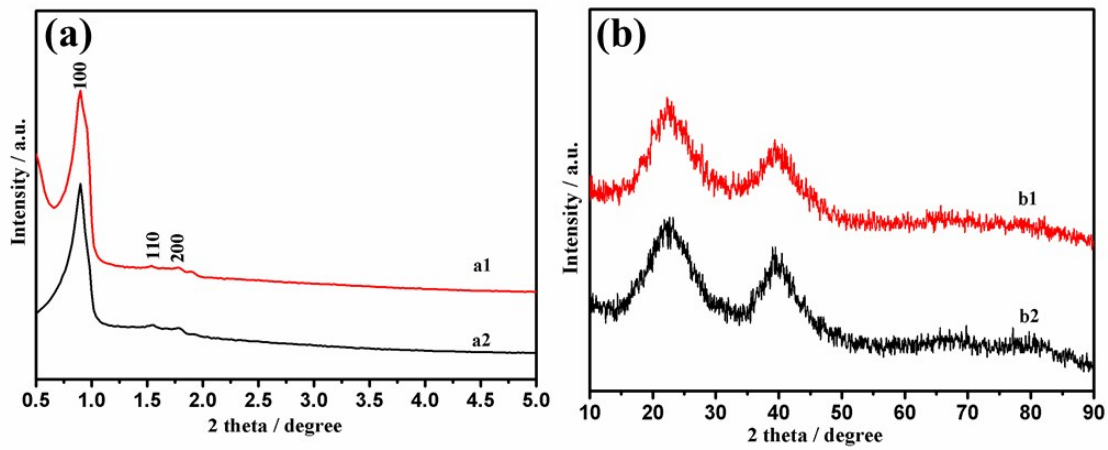

Figure S17. (a) Small-angle XRD patterns and (b) wide-angle XRD patterns for (a1, b1) the $Pd_{0.85}Ir_{0.15}$/SBA-15-NH_2 NCs and (a2, b2) $Pd_{0.85}Ir_{0.15}$/SBA-15-NH_2 NCs after reusability test.

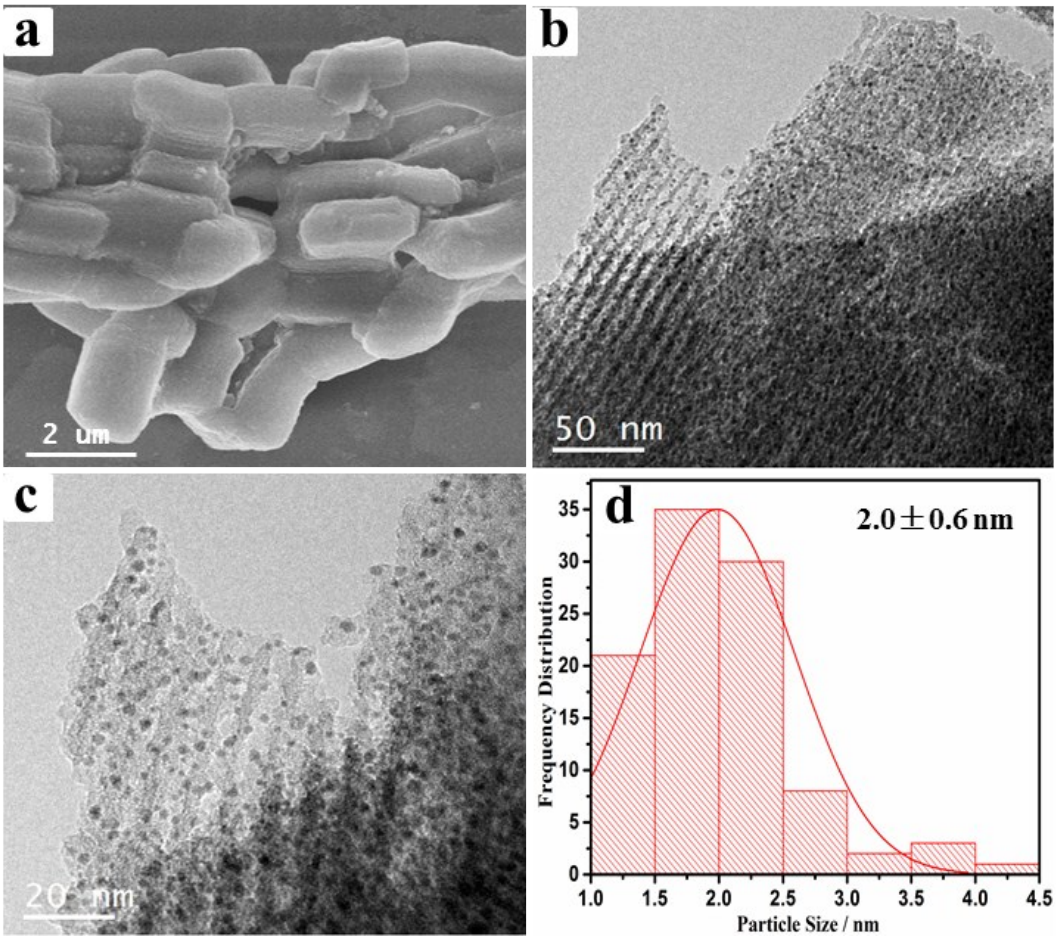

Figure S18. (a) SEM images, (b,c) TEM images, and (d) particle distribution of $Pd_{0.85}Ir_{0.15}$/SBA-15-NH_2 NCs after reusability test.

Table S1 Catalytic activities for the dehydrogenation of formic acid catalyzed by different heterogeneous catalysts.

Catalyst	Temp. (K)	additive	E_a (kJ/mol)	TOF[a] (h^{-1})	Ref.
Without Additive					
$Au_{0.5}Pd_{0.5}/NH_2$-N-rGO	298	None	--	4445.6	S3
$Ag_{0.025}Pd_{0.975}/NH_2$-N-rGO	298	None	--	2556.2	S3
$Pd_{0.85}Ir_{0.15}$/SBA-15-NH_2	298	None	26.7	1500	This work
$Pd_{60}Au_{40}$/ZrSBA-15-AP	298	None	42.5	1185	S4
PdAu-MnO_x/N-SiO_2	298	None	26.2	785	S5
SBA-15-Amine/Pd	299	None		377	S2
CoAuPd/DNA-rGO	298	None		85	S6
AuPd-CeO_2/N-rGO	298	None		52.9	S7
Pd-MnOx/SiO_2-NH_2	323	None		1300	S8
With Additive					
$Pd_{0.85}Ir_{0.15}$/SBA-15-NH_2	298	SF	26.7	3087	This work
Pd@CN900K	298	SF	46.9	1963[b]	S9
$Au_1Pd_{1.5}$/MIL-101-NH_2	298	SF	32.5	526[b]	S10
$Au_{0.28}Pd_{0.47}Co_{0.25}$/MIL-101-$NH_2$	298	SF	32.5	347[b]	S11
Au_2Pd_3@(P)N-C	303	SF	34.8	5400[b]	S12
Pd_1Au_1/72-LA	303	SF	34.4	3583[b]	S13
In situ-Pd@MSC	303	SF	31.7	2965	S14
Pd@SS-CNR	303	SF	38.8	1878[b]	S15
$(Co_6)Ag_{0.1}Pd_{0.9}$/RGO	323	SF	43.1	2739[b]	S16
Au_2Pd_8/SBA-15-Amine	323	SF	47.6	1786	S17
$Pd_{0.58}Ni_{0.18}Ag_{0.24}$/C	323	SF	20.5	85	S18
$Pd_{0.85}Ir_{0.15}$/SBA-15-NH_2	328	SF	26.7	8248	This work
$Pd_{0.6}Ag_{0.4}$@ZrO_2/C/rGO	333	SF	50.1	4500	S19
AuPd@ED-MIL-101	363	SF	--	106	S20
PdAu@Au/C	365	SF	--	59.6	S21

[a] Initial TOF values calculated on initial reaction time or initial conversion of FA.

[b] TOF values calculated on the complete time of gas releasing.

References

[S1] D. Zhao, Q. Huo, J. Feng, B. F. Chmelka and G. D. Stucky, *J. Am. Chem. Soc.,* 1998, **120**, 6024-6036.

[S2] K. Koh, J.-E. Seo, J. H. Lee, A. Goswami, C. W. Yoon and T. Asefa, *J. Mater. Chem. A,* 2014, **2**, 20444-20449.

[S3] S.-J. Li, Y.-T. Zhou, X. Kang, D.-X. Liu, L. Gu, Q.-H. Zhang, J.-M. Yan and Q. Jiang, *Adv. Mater.,* 2019, 1806781.

[S4] Z. Wang, X. Hao, D. Hu, L. Li, X. Song, W. Zhang and M. Jia, *Catal. Sci. Technol.,* 2017, **7**, 2213-2220.

[S5] Y. Karatas, A. Bulut, M. Yurderi, I. E. Ertas, O. Alal, M. Gulcan, M. Celebi, H. Kivrak, M. Kaya and M. Zahmakiran, *Appl. Catal., B,* 2016, **180**, 586-595.

[S6] Z.-L. Wang, H.-L. Wang, J.-M. Yan, Y. Ping, S.-ll. O, S.-J. Li and Q. Jiang, *Chem. Commun.,* 2014, **50**, 2732-2734.

[S7] Z.-L. Wang, J.-M. Yan, Y.-F. Zhang, Y. Ping, H.-L. Wang and Q. Jiang, *Nanoscale,* 2014, **6**, 3073-3077.

[S8] A. Bulut, M. Yurderi, Y. Karatas, M. Zahmakiran, H. Kivrak, M. Gulcan and M. Kaya, *Appl. Catal., B,* 2015, **164**, 324-333.

[S9] Q. Wang, N. Tsumori, M. Kitta and Q. Xu, *ACS Catal.,* 2018, **8**, 12041-12045.

[S10] J. Cheng, X. Gu, P. Liu, H. Zhang, L. Ma and H. Su, *Appl. Catal., B,* 2017, **218**, 460-469.

[S11] J. Chen, X. Gu, P. Liu, T. Wang and H. Su, *J. Mater. Chem. A,* 2016, **4**, 16645-16652.

[S12]Q. Wang, L. Chen, Z. Liu, N. Tsumori, M. Kitta and Q. Xu, *Adv. Funct. Mater.,* 2019, 1903341.

[S13]W. Hong, M. Kitta, N. Tsumori, Y. Himeda, T. Autrey and Q. Xu, *J. Mater. Chem. A,* 2019, **7**, 18835-18839.

[S14]Q.-L. Zhu, F.-Z. Song, Q.-J. Wang, N. Tsumori, Y. Himeda, T. Autrey and Q. Xu, *J. Mater. Chem. A,* 2018, **6**, 5544-5549.

[S15]L. Zou, M. Kitta, J. Hong, K. Suenaga, N. Tsumori, Z. Liu and Q. Xu, *Adv. Mater.,* 2019, 1900440.

[S16]Y. Chen, Q.-L. Zhu, N. Tsumori and Q. Xu, *J. Am. Chem. Soc.,* 2015, **137**, 106-109.

[S17]L. Xu, F. Yao, J. Luo, C. Wan, M. Ye, P. Cui and Y. An, *RSC Adv.,* 2017, **7**, 4746-4752.

[S18]M. Yurderi, A. Bulut, M. Zahmakiran and M. Kaya, *Appl. Catal., B,* 2014, **160-161**, 514-524.

[S19]F.-Z. Song, Q.-L. Zhu, X. Yang, W.-W. Zhan, P. Pachfule, N. Tsumori and Q. Xu, *Adv. Energy Mater.,* 2018, **8**, 1701416.

[S20]X. Gu, Z.-H. Lu, H.-L. Jiang, T. Akita and Q. Xu, *J. Am. Chem. Soc.,* 2011, **133**, 11822-11825.

[S21]Y. Huang, X. Zhou, M. Yin, C. Liu and W. Xing, *Chem. Mater.,* 2010, **22**, 5122-5128.